Kinetic Study of the Reactions of CaO with H_2O, CO_2, O_2, and O_3: Implications for Calcium Chemistry in the Mesosphere

J. M. C. Plane* and R. J. Rollason

School of Environmental Sciences, University of East Anglia, Norwich, NR4 7TJ, United Kingdom

Received: March 1, 2001; In Final Form: May 15, 2001

$CaO(X^1\Sigma^+)$ plays a central role in the atmospheric chemistry of meteor-ablated calcium. A series of CaO reactions was studied by the pulsed photodissociation at 193.3 nm of calcium acetyl acetonate $[Ca(C_5H_7O_2)_2]$ vapor, producing CaO in an excess of reactant and N_2 bath gas. CaO was monitored by time-resolved nonresonant LIF, by pumping the $CaO(B^1\Pi - X^1\Sigma^+)$ transition at 385.9 nm and detecting $B^1\Pi - A^1\Sigma^+$ emission at $\lambda > 693$ nm. The recombination reactions of CaO with H_2O, CO_2, and O_2 were found to be in the falloff region over the experimental pressure range (2−12 Torr). The data were fitted by RRKM theory combined with ab initio quantum calculations on $Ca(OH)_2$, $CaCO_3$ and CaO_3, yielding the following results (180−600 K and $0-10^3$ Torr). For CaO + H_2O, $\log (k_{rec,0}/cm^6\ molecule^{-2}\ s^{-1}) = -23.39 + 1.41 \log T - 0.751 \log^2 T$, $k_{rec,\infty} = 7.02 \times 10^{-10} \exp(-38.4/T)$ $cm^3\ molecule^{-1}\ s^{-1}$, $F_c = 0.31$. For CaO + CO_2: $\log (k_{rec,0}/cm^6\ molecule^{-2}\ s^{-1}) = -36.14 + 9.24 \log T - 2.19 \log^2 T$, $k_{rec,\infty} = 7.97 \times 10^{-10} \exp(-190/T)$ $cm^3\ molecule^{-1}\ s^{-1}$, $F_c = 0.36$. For CaO + O_2: $\log (k_{rec,0}/cm^6\ molecule^{-2}\ s^{-1}) = -42.19 + 13.15 \log T - 2.87 \log^2 T$; $k_{rec,\infty} = 9.90 \times 10^{-10} \exp(-195/T)$ $cm^3\ molecule^{-1}\ s^{-1}$, $F_c = 0.43$ (F_c is the broadening factor). The uncertainty in extrapolating to the mesospheric temperature range (120−250 K) is determined using a Monte Carlo procedure. The reaction between CaO and O_3 is fast with a small T dependence: $k(204-318\ K) = (5.70\ ^{+2.01}_{-1.43}) \times 10^{-10} \exp[(-2.22 \pm 0.62)\ kJ\ mol^{-1}/RT]\ cm^3\ molecule^{-1}\ s^{-1}$, where the quoted uncertainties are at the 95% confidence level. Finally, the implications of these results for calcium chemistry in the mesosphere are discussed.

Introduction

Calcium monoxide (CaO) plays a pivotal role in controlling the layer of atomic Ca that occurs in the Earth's atmosphere between 85 and 95 km.[1] The major source of calcium in this region (the upper mesosphere) is the ablation of the approximately 120 tons of cosmic dust that enters the atmosphere each day.[2,3] The Ca layer can be observed by ground-based resonance fluorescence lidar (laser radar) operating on the atomic Ca transition at 422.0 nm ($Ca(^1P - {}^1S)$).[1,4,5] This has revealed that the Ca layer is depleted by a huge factor of more than 120 with respect to the mesospheric Na layer, when compared to their relative abundances in chondritic meteorites.[1−5] Another unusual feature of the Ca layer is that during summer, when the upper mesosphere is coldest, the abundance of Ca below 90 km actually increases in direct contrast to Na.[1] These very puzzling observations could be explained by Ca ablating less efficiently from meteoroids,[1,3] and through differences in the chemistries that control the formation of the metal atom layers.[1]

We have previously shown that Ca reacts at essentially every collision with O_3 to form CaO.[6] Hence, the next step in unravelling the atmospheric chemistry of calcium is to study the reactions that CaO is likely to undergo at the low temperatures and pressures characteristic of the upper mesosphere:

$$CaO + H_2O + N_2 \rightarrow Ca(OH)_2 + N_2 \quad (1)$$

$$CaO + CO_2 + N_2 \rightarrow CaCO_3 + N_2 \quad (2)$$

$$CaO + O_2 + N_2 \rightarrow CaO_3 + N_2 \quad (3)$$

$$CaO + O_3 \rightarrow CaO_2 + O_2 \quad (4)$$

These reactions are the subject of the present paper. None of them appears to have been studied directly, although the rate coefficient k_1 has been inferred from modeling the behavior of calcium seeded into a flame at about 2000 K.[7] Also, the formation of CaO_3 has been reported in low-temperature matrices where Ca and O_3 were co-condensed.[8,9]

In this paper, we will report an experimental study of reactions 1−4 using a pulsed photolysis/laser-induced fluorescence technique. Besides the application of these reactions to atmospheric chemistry and combustion, they are also of fundamental interest because of the large permanent dipole moment of CaO (8.8 D, vide infra), which can induce a substantial long-range interaction with a potential reactant. The experimental results on these reactions will therefore be complemented by quantum calculations using hybrid density functional/Hartree−Fock theory on the product molecules $Ca(OH)_2$, $CaCO_3$, and CaO_3 (we have previously carried out a detailed theoretical study[10] of the possible geometries and spin states of CaO_2).

In the case of the recombination reactions 1−3, the kinetics will then be modeled using a version of RRKM theory in which

* To whom correspondence should be addressed: E-mail: j.plane@uea.ac.uk. Fax: (44) 1603 507719.

10.1021/jp010810c CCC: $20.00
Published on Web 06/27/2001

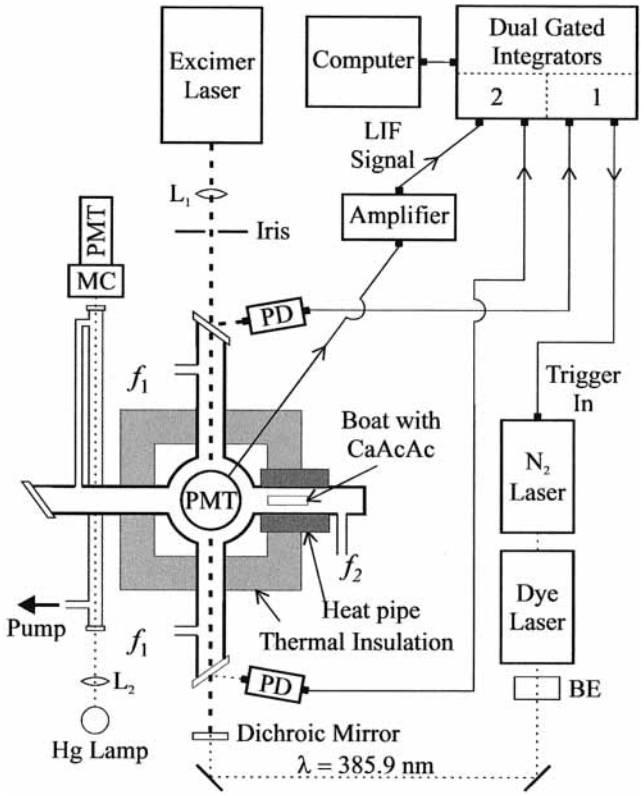

Figure 1. Schematic diagram of the pulsed laser photolysis/laser-induced fluorescence apparatus: **BE**, beam expander; f_1, flow of reagent/bath gas mixture (65 sccm); f_2, CaAcAc dilution flow (100 sccm); L_1, Suprasil lens, $f = 50$ cm; L_2, Suprasil lens, $f = 5$ cm; **MC**, monochromator; **PMT**, photomultiplier tubes; **PD**, fast photodiode.

the microcanonical rate coefficients are calculated using an inverse Laplace transform technique.[11] In addition to the intrinsic interest in understanding the kinetic behavior of these reactions, there is a further practical consideration. The kinetics of these recombination reactions, particularly in the case of reaction 1, will be shown to be significantly in the falloff region at the lowest pressures at which they can be studied by conventional laboratory techniques, such as laser flash photolysis. A theoretical framework is therefore required to extrapolate to the much lower pressures of the upper mesosphere (10^{-5} to 10^{-6} atmospheres).

Experimental Section

Figure 1 is a schematic diagram of the pulsed laser photolysis/laser-induced fluorescence (PLP/LIF) apparatus used to study these reactions. CaO was produced in the central chamber of the stainless steel reactor by the pulsed multiphoton photolysis of calcium acetyl acetonate (CaAcAc, $Ca(C_5H_7O_2)_2$) in an excess of the reactant (O_2, O_3, CO_2 or H_2O) and bath gas (N_2). Powdered CaAcAc was placed in a tantalum boat located inside the heat pipe attached to the central chamber. The heat pipe temperature was then set in the range 438−473 K, and maintained to within ± 2 K during an experiment. The resulting CaAcAc vapor was entrained in a small flow of N_2 bath gas and carried into the central chamber, where it mixed with larger flows of the N_2 bath gas and a reactant/N_2 bath gas mixture. Photolysis of CaAcAc vapor at 193.3 nm using an ArF excimer laser (pulse energy ≈ 50 mJ) produced both Ca and CaO. For the study of reaction 4, the estimated fluence of excimer radiation in the chamber was $\approx 3 \times 10^{16}$ photon cm^{-2}, so that less than 1% of O_3 would have been photolyzed.

CaO was probed at 385.9 nm [$CaO(B^1\Pi - X^1\Sigma^+)$, $A_{nm} = 3.1 \times 10^7\ s^{-1}$ [12]] using a nitrogen-pumped dye laser (laser dye BBQ, pulse energy 20 μJ; bandwidth = 0.04 nm). The nonresonant LIF signal at $\lambda > 693$ nm [$CaO(B^1\Pi - A^1\Sigma^+)$] was detected by a photomultiplier tube (PMT) after passing through a cut-on filter at 645 nm. The relatively weak LIF signal was then amplified (Stanford Research Systems, model SR445 DC-300 MHz) and collected by a gated integrator with a 40 ns wide gate. As shown in Figure 1, a second gated integrator, triggered by the excimer laser pulse, was used to trigger the probe laser after a scanned time delay controlled by a microcomputer. The excimer laser and dye laser beams were aligned collinearly to pass through the center of the chamber, with the dye laser protected from the excimer beam by a dichroic reflector.

For reaction 4, the concentration of O_3 was monitored downstream of the reactor by optical absorption of the 253.7 nm emission line from a low-pressure mercury lamp. The absorption cross section was taken as 1.143×10^{-17} cm^2 at 298 K.[13] For reaction 1, wall losses of H_2O were minimized by allowing each new flow of H_2O in N_2 at least 5 min to equilibrate with the walls of the reactor and checking that the observed first-order loss of CaO did not change at longer times.

Materials. N_2 and O_2, 99.9999% pure (Air products), and CO_2 99.995% pure (Air Products) were used without further purification. Milli-Q H_2O was freeze−pump−thawed for several cycles in a glass handling line, and H_2O vapor then made up to a known ratio in about 760 Torr of bath gas in a glass bulb. O_3 was made by flowing O_2 through a commercial ozonizer. The resulting 5−8% O_3/O_2 mixture was collected on silica gel held at 156 K. O_2 was then pumped off at 195 K until a >40% O_3/O_2 mixture degassed from the gel. CaAcAc, 98% pure (Johnson Matthey), was further purified by being pumped on in the heat pipe at ∼400 K for an hour prior to experiments.

Results

CaO was formed directly on photolysis of CaAcAc, without requiring the presence of an oxidant (cf. our recent studies of FeO reaction kinetics[14,15]). Figure 2a illustrates two time-resolved decays of the LIF signal from CaO. The smaller signal, which decays more slowly, was recorded in the absence of a reactant, with only the bath gas and CaAcAc in the reactor. The second decay shown in Figure 2a was recorded on the same scale as the first, but now with O_2 added. This shows that not only did the decay rate increase because of reaction 3, but also the LIF signal was considerably enhanced. This indicates that CaAcAc reacts with O_2 to form a photolytic precursor of CaO. This phenomenon was not observed when H_2O or CO_2 was added.

In the case of reactions 1−3, where the reagent R (= H_2O, CO_2 or O_2) was in a large excess over CaO, the removal of CaO should be described by the pseudo first-order decay coefficient

$$k' = k_{\text{diff, CaO}} + k_{\text{CaAcAc}}[\text{CaAcAc}] + k_{\text{rec}}[\text{R}] \qquad \text{(I)}$$

where the term $k_{\text{diff, CaO}}$ describes the diffusion of CaO out of the volume defined by the dye laser beam and within the field of view of the PMT; k_{CaAcAc} is the rate of an apparent reaction between CaO and the CaAcAc precursor; and k_{rec} is the second-order rate coefficient for the recombination reactions 1, 2, or 3 at a particular pressure (i.e., k_1, k_2 or k_3, respectively). As expected, the LIF decays were well fitted by a single exponential form, shown by the solid lines in Figure 2a; the residuals to the

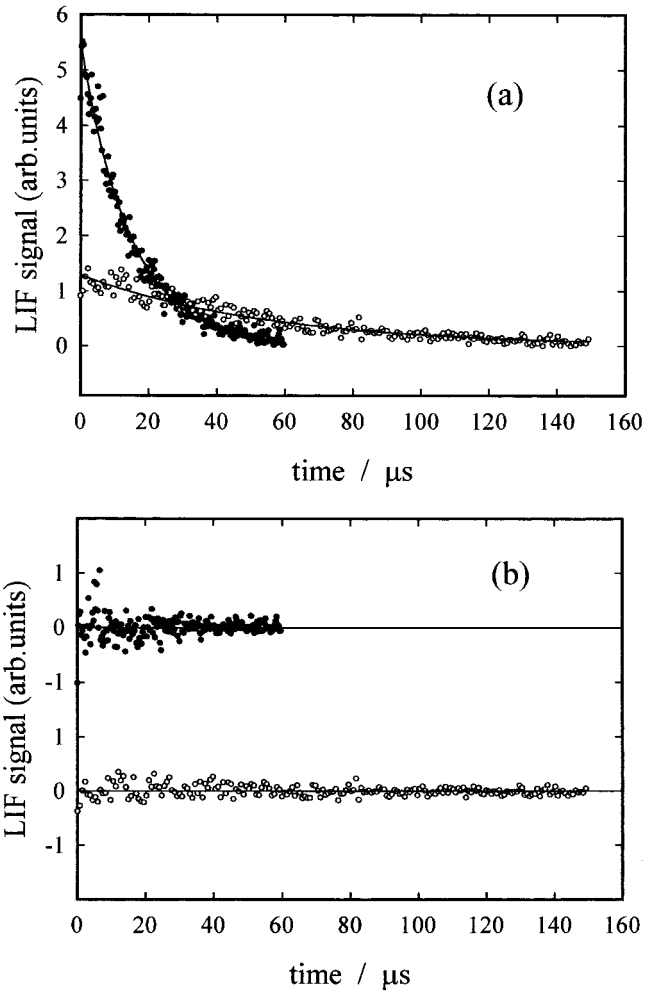

Figure 2. Time-resolved decays of the laser-induced fluorescence (LIF) signal from CaO probed at 385.5 nm [CaO($B^1\Pi - X^1\Sigma^+$) and detected by the nonresonant LIF signal [CaO($B^1\Pi - A^1\Sigma^+$)] at 693 nm. (a) LIF decays without O_2 (slower decay) and $[O_2] = 3.48 \times 10^{15}$ molecules cm^{-3}, $[N_2] = 6.61 \times 10^{16}$ molecules cm^{-3}, $T = 483$ K. The solid curves are fits of the form $A\exp(-k't)$ to the data points, yielding $k' = 20\,580$ and 68 670 s^{-1} respectively. (b) Plots of the residuals between the data-points and the fitted curves from (a). Note that the LIF signal is greatly enhanced by the presence of O_2.

fits are plotted in Figure 2b. Data sets were obtained by measuring k' as a function of [R] at constant pressure and temperature in the central chamber and heat pipe. Thus, $k_{diff,CaO} + k_{CaAcAc}[CaAcAc]$ appeared as the intercept in a plot of k' vs [R]. These intercepts ranged from 6100 to 74 000 s^{-1}. Indeed, the occurrence of a reaction between CaO and CaAcAc is inferred from these large intercepts, which were a function of the temperature in the heat pipe, and hence, the vapor pressure of CaAcAc entering the central chamber. Figure 3 shows examples of k' vs $[CO_2]$ for reaction 2. The slopes of plots of this type yielded k_{1-3} as a function of temperature and pressure, listed in Tables 1−3. Figure 4a shows the pressure dependences (over a factor of ~4) of k_{1-3} at close to room temperature. Reaction 1 exhibits no pressure dependence over the range 2.9−8.2 Torr, and reactions 2 and 3 are clearly well into the falloff region. The upper temperature limit for studying these reactions was about 500 K, above which the thermal decomposition of CaAcAc became too rapid. The lower temperature limit for reaction 1 was 278 K because of significant condensation of H_2O on the reactor walls at lower temperatures. The lower limit for reaction 2 of 213 K was likewise constrained by condensation of CO_2, whereas reaction 3 was measured down to 199 K,

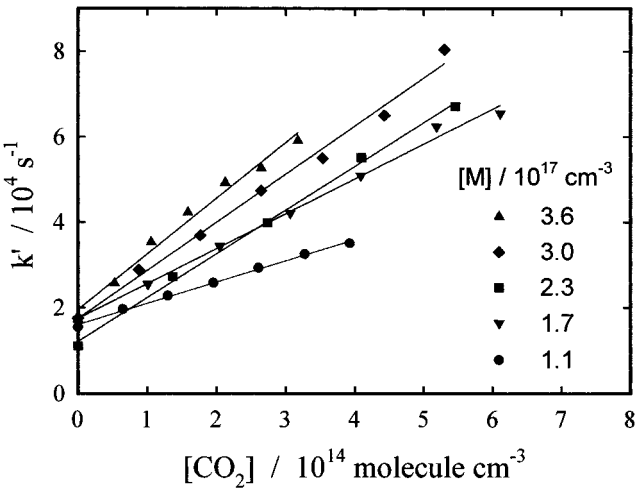

Figure 3. k' vs. $[CO_2]$ for the recombination reaction between CaO and CO_2 in N_2 bath gas, as a function of third body concentration [M] at 311 K. The solid lines are linear regression fits through each set of data.

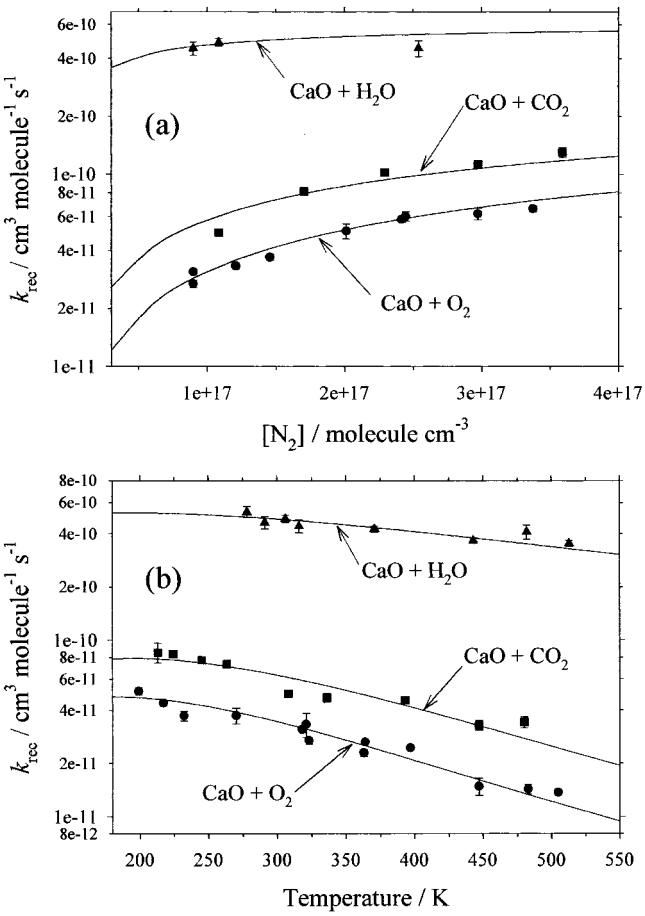

Figure 4. (a) k_{rec} vs [M], demonstrating that reactions 1−3 are in the falloff pressure region. These data are close to room temperature (306−323 K) (b) k_{rec} vs temperature, for pressures between 2.9 and 3.9 Torr. The individual rate coefficients are plotted with the 1σ standard errors from linear regression fits to kinetic plots of the type illustrated in Figure 3. The solid curves are fits of RRKM theory to the data (at a pressure of 3.5 Torr in (b)).

a limit imposed by cooling the reactor with solid CO_2. Figure 4b shows that all three reactions have small negative temperature dependences.

The 1σ uncertainties in k_{1-3}, obtained from the standard errors to the slopes of kinetic plots exemplified in Figure 3, are

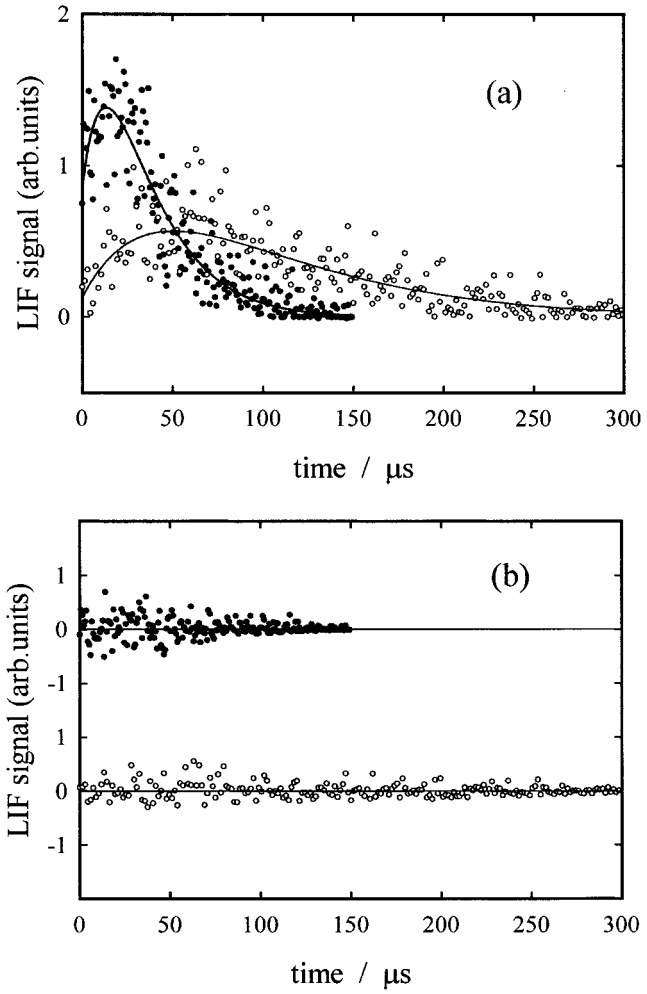

Figure 5. Time-resolved decays of the laser-induced fluorescence (LIF) signal from CaO probed at 385.9 nm [CaO($B^1\Pi - X^1\Sigma^+$) and detected by the nonresonant LIF signal [CaO($B^1\Pi - A^1\Sigma^+$)] at > 693 nm. (a) LIF decays with $[O_3] = 2.28 \times 10^{13}$ molecules cm^{-3} (faster decay) and $[O_3] = 1.21 \times 10^{14}$ molecules cm^{-3}, $[N_2] = 8.60 \times 10^{16}$ molecules cm^{-3}, $T = 313$ K. The solid curves are fits of eq II to the data points, yielding $k_4' + k_{diff,CaO} = 14\,500$ and $37\,000$ s^{-1} respectively. (b) Plots of the residuals between the data-points and fitted curves from (a).

listed in Tables 1−3 and plotted in Figure 4. The reproducibility of these second-order rate coefficients is estimated to be ± 20%. This is based on the scatter of the experimental data points about the RRKM fits (see below), which are shown as solid lines in Figure 4, and corresponds roughly to the largest 2σ uncertainties in the experimental data points. The absolute uncertainties are estimated to be ± 22%, which combines in quadrature the 20% statistical error with a 10% systematic error, comprising the sum of the uncertainties in the flow controllers (5%), the reactor pressure (4%) and the temperature (1%).

When studying reaction 4, some initial growth in CaO was observed following photolysis in the presence of O_3 (Figure 5). This is because Ca, which is also produced when CaAcAc is photolyzed,[6,16] reacts with O_3 to form CaO

$$Ca + O_3 \rightarrow CaO + O_2 \qquad (5)$$

A further potential complication is that O_2 is present in the reactor from the O_3/O_2 mixture, so that reaction 3 and the recombination reaction

$$Ca + O_2 + N_2 \rightarrow CaO_2 + N_2 \qquad (6)$$

TABLE 1: Experimental Determination of k_1(CaO + H_2O) as a Function of Temperature and Pressure of N_2 (Quoted Uncertainty is 1σ)

T/K	pressure/Torr	$k_1/10^{-10}$ cm^3 molecule^{-1} s^{-1}
278	2.9	5.31 ± 0.38
291	2.9	4.63 ± 0.37
306	3.5	4.86 ± 0.23
310	8.2	4.53 ± 0.43
316	2.9	4.41 ± 0.36
371	3.5	4.25 ± 0.17
443	3.5	3.66 ±_ 0.13
482	2.9	4.09 ±_ 0.37
513	3.8	3.53 ±_ 0.14

TABLE 2: Experimental Determination of k_2(CaO + CO_2) as a Function of Temperature and Pressure of N_2 (Quoted Uncertainty is 1σ)

T/K	pressure/Torr	$k_2/10^{-11}$ cm^3 molecule^{-1} s^{-1}
213	3.1	8.51 ± 1.09
224	3.6	8.32 ± 0.23
245	4.0	7.70 ± 0.29
263	3.9	7.29 ± 0.29
308	3.5	4.97 ± 0.12
309	5.5	8.17 ± 0.27
311	7.4	10.23 ± 0.29
312	9.6	11.26 ± 0.47
314	11.6	13.00 ± 0.77
336	2.9	4.72 ± 0.28
393	3.6	4.55 ± 0.15
447	3.6	3.28 ± 0.22
480	2.8	3.43 ± 0.26

TABLE 3: Experimental Determination of k_3(CaO + O_2) as a Function of Temperature and Pressure of N_2 (Quoted Uncertainty is 1σ)

T/K	pressure/Torr	$k_3/10^{-11}$ cm^3 molecule^{-1} s^{-1}
199	3.6	5.12 ± 0.25
217	3.6	4.40 ± 0.33
232	3.6	3.72 ± 0.17
270	3.6	3.73 ± 0.23
316	4.7	3.70± 0.22
316	7.9	6.05± 0.39
318	2.9	3.11± 0.13
320	6.5	5.06± 0.34
321	3.9	3.33 ± 0.10
322	9.6	6.23 ± 0.46
322	10.9	6.62 ± 0.52
323	7.8	5.82 ± 0.44
323	2.9	2.69 ± 0.23
363	3.6	2.29 ± 0.18
364	3.4	2.64 ± 0.12
397	3.6	2.45 ± 0.10
447	3.5	1.48 ± 0.05
483	3.5	1.43 ± 0.04
505	3.9	1.37 ± 0.16

could play a significant role. However, k_3 was measured in this study (Table 3) and k_6 has been measured previously.[10,16] At the relatively low N_2 concentrations employed, the contributions of these reactions to the removal of CaO and Ca were less than $15\,000$ s^{-1} and 120 s^{-1}, respectively.

The time-resolved LIF profiles of CaO were therefore fitted to a linear combination of exponential decays

$$[CaO] = a[Ca]_0(e^{-bt} - e^{-ct}) + [CaO]_0e^{-ct} \qquad (II)$$

where $[Ca]_0$ and $[CaO]_0$ are the concentrations formed directly on photolysis. The adjustable parameters are $a = k_5'/((k_4' + k_3' + k_{CaO,diff}) - (k_5' + k_6' + k_{Ca,diff}))$, $b = (k_5' + k_6' + k_{Ca,diff})$ and $c = (k_4' + k_3' + k_{CaO,diff})$, where the rates of diffusion of Ca, $k_{Ca,diff}$, and of CaO, $k_{CaO,diff}$, ranged from 2500 s^{-1} to 17 000

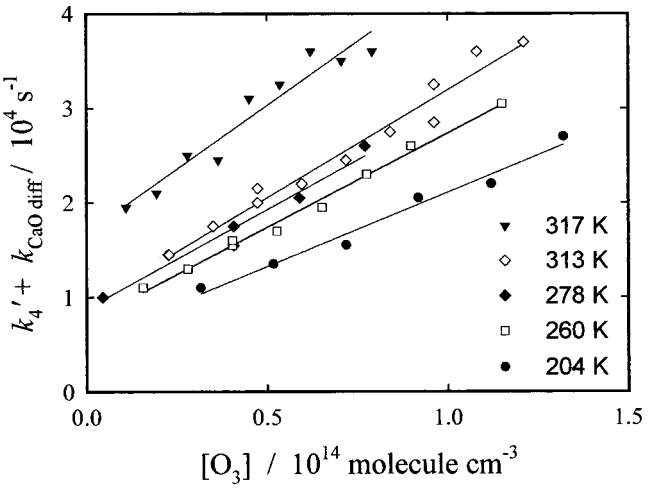

Figure 6. $k_4' + k_{\text{diff CaO}}$ vs $[O_3]$ for the reaction CaO + O_3 at five temperatures. The solid lines are linear regression fits through each set of data.

TABLE 4: Experimental Determination of k_4 (CaO + O_3) as a Function of Temperature (Quoted Uncertainty is 1σ)

T/K	pressure/Torr	$k_4/10^{-10}$ cm^3 molecule^{-1} s^{-1}
204	2.8	1.57 ± 0.12
216	2.8	1.70 ± 0.08
230	2.8	1.71 ± 0.09
278	2.8	2.10 ± 0.21
313	2.8	2.28 ± 0.14
317	2.8	2.70 ± 0.28
318	7.9	2.48 ± 0.24

s^{-1}. Note that the reactions of Ca and CaO with CaAcAc are now folded into these diffusion terms. k_3', k_4', k_5', and k_6' are the first-order rate coefficients for reactions 3−6, respectively.

The ratio $[CaO]_0$:$[Ca]_0$ varied from about 1:19 to 1:3, depending on the O_3 concentration. Figure 5 illustrates two time-resolved decays of the LIF signal from CaO in the presence of different concentrations of O_3. The initial LIF signal is larger when there is more O_3 present. Because the O_3 was in fact a mixture of ~40% O_3 in O_2, CaAcAc would have reacted with O_2 (vide supra), and probably also with O_3, to form a photolytic precursor of CaO. Note that the LIF signals in Figure 5 are somewhat noisier than in Figure 2—this is because lower excimer laser fluences were employed to limit the photolysis of O_3 in the reactor.

The parameters $a-c$ in eq II were optimized in a computer model to best fit the LIF profiles, as illustrated in Figure 5. Plots of $k_4' + k_{\text{CaO,diff}}$ vs $[O_3]$ are shown in Figure 6, for a selection of temperatures. The slopes of these plots therefore yield k_4, listed as a function of temperature in Table 4. The resulting Arrhenius plot in Figure 7 yields

$$k_4 = (5.70\ ^{+2.01}_{-1.43}) \times 10^{-10} \exp((-2.22 \pm 0.62)\ \text{kJ mol}^{-1}/RT)\ \text{cm}^3\ \text{molecule}^{-1}\ \text{s}^{-1} \quad \text{(III)}$$

with the overall uncertainty in k_4 at the 95% confidence level given by

$$\sigma(k_4) = k_4[5300/T^2 - 41/T + 0.081]^{0.5}$$

The upper temperature limit for this reaction was 318 K because the decomposition of O_3 at higher temperatures became significant, probably as a result of thermal wall losses and reaction with CaAcAc.

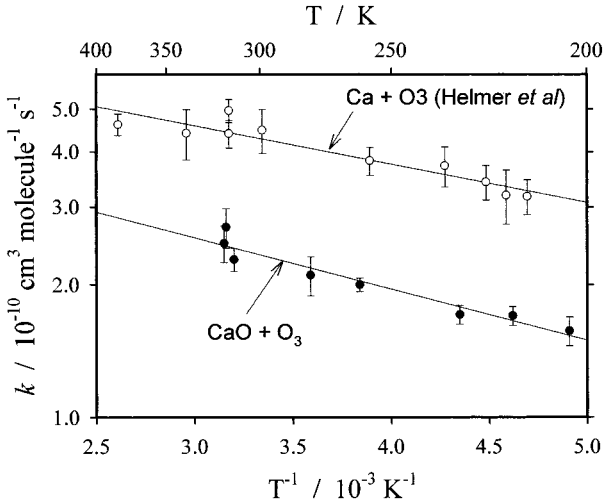

Figure 7. Arrhenius plot for the reaction between CaO and O_3. The individual rate coefficients are plotted with the 1σ standard errors from linear regression fits to kinetic plots of the type illustrated in Figure 6. The solid line is a linear regression fit through the experimental points. Also shown is the Arrhenius plot for Ca with O_3, studied by Helmer et al.[6]

Ab Initio Quantum Calculations

To interpret these experimental results, a set of quantum calculations was performed on the calcium-containing species involved in reactions 1−4. The hybrid density functional/Hartree−Fock B3LYP method was employed from within the Gaussian 98 suite of programs,[17] combined with the 6-311+G-(2d,p) triple-ζ basis set. This is a large, flexible basis set which has both polarization and diffuse functions added to the atoms.[17] At this level of theory, the expected uncertainty in the calculated reaction enthalpies is ±14 kJ mol^{-1}.[18] The geometries of CaO, CaOH, $Ca(OH)_2$, $CaCO_3$, and CaO_3 were first optimized, checked for wave function stability, and their respective vibrational frequencies calculated. In the case of CaO_3, two isomeric forms were explored: the trioxide $OCaO_2$, where only the triplet wave function would converge; and the ozonide CaO_3, where both singlet and triplet calculations were performed.

Figure 8 illustrates the geometries of these molecules. Their calculated dipole moments, rotational constants and vibrational frequencies are listed in Table 5. In the case of CaO($X^1\Sigma^+$) and CaO($a^3\Pi$), the theoretical bond lengths, vibrational frequencies and relative energies are in excellent agreement with experiment (Table 5). The calculated bond energy of CaO(X), $D_0(\text{Ca}-\text{O}) = 415 \pm 14$ kJ mol^{-1}, is in satisfactory agreement with a fairly recent experimental estimate of 399 ± 8 kJ mol^{-1}.[20] There is also excellent agreement between the theoretical and experimental vibrational frequencies, dipole moment and heat of formation of CaOH.

CaO_3 has been observed in inert gas matrices by co-condensing both Ca with O_3,[8] and excited Ca atoms with O_2.[9] Our calculated vibrational frequencies indicate that singlet CaO_3 was formed in these matrix experiments (which would conserve spin). The lowest observed frequency at 426 cm^{-1} is the $Ca^+-O_3^-$ interionic stretch;[8] a band at 634 cm^{-1} arises from the ν_2 asymmetric stretch of O_3^-;[9] and a band at 804−806 is the ν_3 symmetric stretch of O_3^-.[8,9] Our corresponding theoretical frequencies are 4−9% higher (Table 5), which is very good agreement considering that the matrix environment will cause small shifts in frequencies compared to the isolated gas phase. Furthermore, the experimental O−O−O bond angle[8] of 114 ± 6° is in good accord with the present calculated value of 109.1°. Thus, the theoretical method we have employed here appears

TABLE 5: Calculated Molecular Parameters and Heats of Formation for CaO($X^1\Sigma^+$ and $a^3\Pi$), CaOH, $Ca(OH)_2$, $CaCO_3$, and CaO_3 at the B3LYP/6-311+G(2d,p) Level of Theory[r]

species (see Figure 8)	dipole moment[a]	rotational constants[b]	vibrational frequencies[c]	$\Delta H^{o}_{f,0}$ [d]
CaO ($X^1\Sigma^+$)	8.76	13.4 [13.3 [e]]	780 [733 [e]]	9.1 [f] [25.1 [g]]
CaO ($a^3\Pi$)	3.56	10.23 [10.21 [e]]	532 [556 [e]]	102.4 [122.0 [e,g]]
Ca(OH)($^2\Sigma^+$) linear	1.08 [1.47 [h]]	10.07 [10.10 [i]]	350 (x2) [353 [j]] 615 [609 [j]] 3959 [3847 [k]]	−176.8 [−190.0 [e], −176.3[g]]
$Ca(OH)_2$ (^{1}A′) planar, C_{2v}	1.47	204.7, 3.45, 3.39	69, 419, 422 (x2), 424, 531, 615 [592 [l]], 3960 (×2)	−608.0 [m] [−603.2 [e], −605 [g]]
$Ca(OH)_2$($^1\Sigma^+$) linear	0.0	3.33	51.2*i* (x2), 435 (x4), 518, 610 [592 [l]], 3956 (x2)	−608.0 [m]
$CaCO_3$ (^{1}A′) planar, C_{2v}	13.5	12.62, 2.81, 2.30	119, 363, 453, 656, 762, 828, 951, 1084, 1754	−614.7 [m]
$OCaO_2$ (^{3}A′) C_2 symmetry	3.02	27.35, 2.54, 2.41	61, 73, 398, 399, 527, 1181	−187.7 [m]
CaO_3(^{1}A′) C_2 symmetry	10.1	9.66, 6.40, 4.23	293, 416, 464 [426 [n]], 607 [634 [p]], 693, 855 [804 [n], 807 [p]]	−126.3 [q]
CaO_3($^3B_1$) planar, C_{2v}	2.58	12.58, 4.35, 3.23	162, 260, 325, 662, 879, 1080	−23.3 [m]

[a] In Debye (= 3.336×10^{-30} Cm). [b] In GHz. [c] In cm^{-1}. [d] In kJ mol^{-1}, theoretical uncertainty = ± 14 kJ mol^{-1}. [e] ref 19. [f] Using ab initio D_0(Ca−O) = 414.9 kJ mol^{-1} at the B3LYP/6-311+G(2d,p) level. [g] Using experimental D_0(Ca−O) = 399 ± 6 kJ mol^{-1} from ref 20. [h] ref 21. [i] ref 22. [j] ref 23. [k] ref 24. [l] ref 25. [m] Calculated via isogyric reaction with H_2 (see text), using $\Delta H^{o}_{f,0}$(CaO) = 25.1 kJ mol^{-1}. [n] ref 8. [p] ref 9. [q] Calculated from $\Delta H^{o}_{f,0}(OCaO_2)$. [r] For comparison, experimental values (where available) are shown in parentheses.

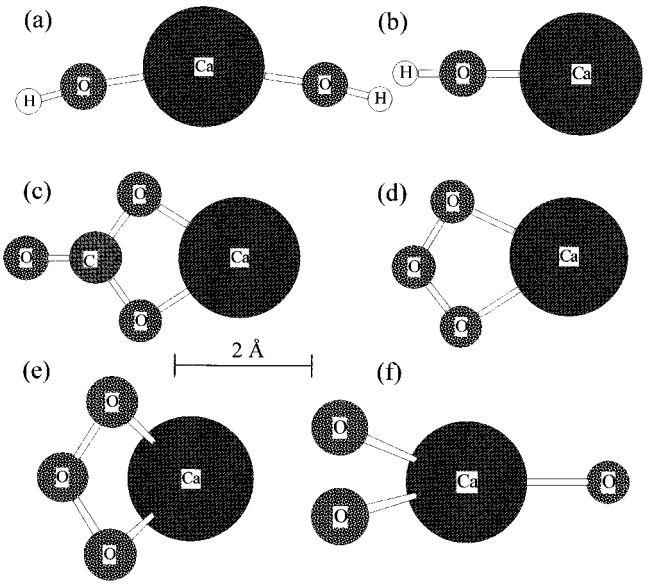

Figure 8. Geometries of (a) $Ca(OH)_2$, (b) CaOH, (c) $CaCO_3$, (d) CaO_3($^3B_1$), (e) CaO_3(^{1}A′) and (f) $OCaO_2$(^{3}A′), determined at the B3LYP/6-311+G(2d,p) level of theory. Note that species (c) and (d) are planar; (e) and (f) have C_2 symmetry, with dihedral angles of 124.0° and 74.3° viewed along the Ca−O mirror plane.

to perform satisfactorily. We are also in sensible accord with previous theoretical work on CaO, CaOH and CaO_3 by Bauschlicher and co-workers.[9,26,27]

There does not appear to be any experimental work on $CaCO_3$ in the gas phase. However, P. D. Siders (U. of Minnesota, Pers. comm.) has followed up his recent theoretical study[28] on $CaCO_3$ with a higher level calculation on the enthalpy change for reaction 2, using second-order Møller−Plesset theory and the Ahlrichs triple-ζ valence basis set. This yields ΔH_0(CaO + CO_2 → $CaCO_3$) = −243 kJ mol^{-1}, which compares very well with −247 kJ mol^{-1} from the present calculations. In the case of $Ca(OH)_2$, the molecule is slightly bent (Figure 8) with a very low-frequency bending motion of the two OH groups about the central Ca atom. This motion transforms into two small imaginary frequencies if the molecule is constrained to be linear (Table 5).

The heats of formation for CaO_3, $CaCO_3$, and $Ca(OH)_2$ listed in Table 5 were then calculated from the enthalpy changes for a set of isogyric reactions with H_2 e.g., $Ca(OH)_2 + H_2 \rightarrow Ca + 2H_2O$. The resulting theoretical estimate for $\Delta H_{f,0}{}^{o}(Ca(OH)_2)$ is in excellent agreement with the value listed in the JANAF tables[19] (Table 5), and a more recent estimate from flame studies.[7,20]

Discussion

CaO + O_3. The bond energy of CaO is 399 ± 8 kJ mol^{-1}.[20] The two most stable forms of the product CaO_2 are the $^1A_1$ and $^3A_2$ superoxides, where the bond energies D_0(Ca−O_2) are 229 ± 14 and 195 ± 14 kJ mol^{-1}, respectively.[10] Hence, reaction 4 is quite exothermic: if the reaction is adiabatic with respect to spin then $\Delta H_0{}^{o}(4) = -189$ or −129 kJ mol^{-1} to form CaO_2-($^3A_2$) + O_2($^3\Sigma_g^-$) or CaO_2($^1A_1$) + O_2($^1\Delta_g$), respectively. Note that the alternative reaction pathway to produce Ca + $2O_2$ is endothermic by 6 ± 8 kJ mol^{-1}, and is thus unlikely to compete with reaction 4.

The rate coefficient for reaction 4 is characterized by a very small temperature dependence and large preexponential factor (eq III). As shown in Figure 7, its temperature dependence is very similar to that of reaction 5, Ca + O_3. k_4 can also be compared with the collision frequency calculated by applying the orbiting criterion.[15] This requires that successful collisions between CaO and O_3 must surmount the centrifugal barrier on the effective potential, in this case governed by the C_6/R^6 potential[29]

$$C_6 \approx C_6^{\text{disp}} + C_6^{\text{ind}} + C_6^{\text{d-d}} \qquad \text{(IV)}$$

where the dispersion coefficient, C_6^{disp}, the dipole−induced dipole coefficient, C_6^{ind}, and the interaction between the permanent dipoles of the collision partners, $C_6^{\text{d-d}}$, can be estimated using analytical expressions that we have given elsewhere.[15] The relevant molecular parameters are listed in Table 6. Because CaO has a very large permanent dipole

TABLE 6: Molecular Parameters for Collision Frequency Calculations

parameter	CaO	O_3
dipole moment/Debye[a]	8.8[b]	0.53[c]
polarizability/10^{-24} cm^3	6.6[b]	3.21[c]
ionization energy/eV	6.9[d]	12.43[e]

[a] 1 $D = 3.336 \times 10^{-30}$ Cm. [b]Calculated at the B3LYP/6-311+G(2d,p) level of theory (see text). [c]ref 30. [d]ref 31. [e]ref 32.

moment, the three terms in eq IV are comparable in size: $C_6^{disp} = 2.3 \times 10^{-23}$, $C_6^{ind} = 2.5 \times 10^{-23}$, and C_6^{d-d} range from 2.5×10^{-23} to 5.1×10^{-23} J molecule^{-1} nm^6 over the experimental temperature range of 200 to 400 K. The resulting collision frequency[15] over this temperature range is 7.2×10^{-10} cm^3 molecule^{-1} s^{-1}, almost independent of T. Comparison with Figure 7 shows that this collision frequency is indeed an upper limit to k_4, by a factor of between 2.5 and 4.8 over the experimental temperature range.

CaO + H_2O, CO_2 and O_2. The enthalpy changes (at 0 K) for the recombination of CaO with H_2O, CO_2 and O_2 are −394, −247 and −188 kJ mol^{-1}, respectively, calculated from the data in Table 5. As shown in Figure 4, the rate coefficients k_{1-3} decrease in the same order as these reaction exothermicities. Figure 4 also reveals that all three reactions are well into the falloff region. Therefore, to extrapolate the rate coefficients outside the pressure and temperature regimes that were accessible with the experimental technique used in this study, we now apply RRKM theory using the Master Equation (ME) formalism developed by De Avillez Pereira et al.[11]

We have recently described the application of this formalism to recombination reactions of metallic species,[10,15] so only a brief description is given here. The reactions are assumed to proceed via the formation of an excited adduct ($Ca(OH)_2$*, $CaCO_3$* or $OCaO_2$*), which can either dissociate or be stabilized by collision with the third body (N_2). The energy of the adduct was therefore divided into a contiguous set of grains (width 30 cm^{-1}), each containing a bundle of rovibrational states. Each grain was then assigned a set of microcanonical rate coefficients for dissociation, which were determined using inverse Laplace transformation to link them directly to $k_{rec,\infty}$, the high-pressure limit recombination coefficient.[11] In the present case, $k_{rec,\infty}$ was expressed in the Arrhenius form $A^\infty \exp(-E^\infty/RT)$.

The densitiy of states of the adduct was calculated using a combination of the Beyer−Swinehart algorithm[33] for the vibrational modes (without making a correction for anharmonicity) and a classical densities of states treatment for the rotational modes. The molecular parameters listed in Table 5 were used. In the case of reaction 2, the lowest frequency vibrational mode (119 cm^{-1}) was treated as a free 1-dimensional rotor between CaO and CO_2. Reaction 3 was assumed to occur on a triplet surface to form $OCaO_2$(^{3}A'), and the two lowest frequency modes (61 and 72 cm^{-1}) were treated as a 2-dimensional free rotor between CaO and O_2.

The ME describes the evolution with time of the grain populations of the adduct. The probability of collisional transfer between grains was estimated using the exponential down model,[33] where the average energy for downward transitions, $\langle\Delta E\rangle_{down}$, was an adjustable parameter between 150 and 500 cm^{-1} for N_2 at 250 K. The probabilities for upward transitions were calculated by detailed balance. To use the ME to simulate irreversible stabilization of the adduct, an absorbing boundary was set 24 kJ mol^{-1} below the energy of the reactants, so that collisional energization from the boundary to the threshold was highly improbable.

TABLE 7: Fitted Parameters for the RRKM Calculations on Reactions 1−3 (M = N_2)

parameter reaction	A^∞ cm^3 molecule^{-1} s^{-1}	E^∞ kJ mol^{-1}	$\langle\Delta E\rangle_{down}$[a] cm^{-1}	α	σ Å	ϵ/k K
$CaO + H_2O$	7.02×10^{-10}	0.32	288	1.8	4.5	450
$CaO + CO_2$	7.97×10^{-10}	1.58	190	2.5	4.0	400
$CaO + O_2$	9.90×10^{-10}	1.62	497	2.9	5.0	500

[a] At 250 K.

The ME was expressed in matrix form[11] and then solved to yield k_{calc}, the recombination rate constant at a specified pressure and temperature. To fit k_{calc} to the experimental data in Tables 1−3, six adjustable parameters were allowed. These were the Arrhenius parameters A^∞ and E^∞ which define $k_{rec,\infty}$; the average energy for downward transitions, $\langle\Delta E\rangle_{down}$; α, which defines the T^α dependence of $\langle\Delta E\rangle_{down}$; and σ and ϵ/k which describe the intermolecular potential between the adduct and the N_2, used to calculate their collision frequency.[34] These parameters were varied in a simple grid search to minimize χ^2, defined as

$$\chi^2 = \sum_i^N \left(\frac{k_{meas,i} - k_{calc,i}}{\sigma_i} \right)^2 \qquad \text{(V)}$$

i.e., the sum over N experimental points of the squared difference between the measured $k_{meas,i}$ (with uncertainty σ_i) and the modeled value $k_{calc,i}$. The best fit parameters are listed in Table 7. The large values of A^∞ and the modest activation energies E^∞ are consistent with $k_{rec,\infty}$ being controlled by long-range forces governed by the very large dipole moment and relatively large polarizability of CaO (Table 6).

The largest deviation between k_{calc} and k_{meas} was 46%, with an average deviation of 7%. The satisfactory fits of RRKM theory to the experimental data for reactions 1 to 3 over a range of pressure and temperature is illustrated in Figure 4.

To provide simple expressions for extrapolating k_{calc} for reactions 1−3 over a large range of temperature (120−600 K) and pressure (0−1000 Torr), we have expressed the T dependence of $k_{rec,0}$, the (third-order) rate coefficient at the low-pressure limit, as a 2nd-order polynomial in log T, and then fitted the theoretical results for each reaction to the Lindemann expression modified by a broadening factor F_c[17,29]

$$k_{calc} = \frac{k_{rec,0}[M]}{1 + \frac{k_{rec,0}[M]}{k_{rec,\infty}}} F_c^{\,K}, \text{ where } K = \frac{1}{\left\{1 + \left(\log_{10}\left(\frac{k_{rec,0}[M]}{k_{rec,\infty}}\right)\right)^2\right\}} \qquad \text{(VI)}$$

The resulting fits are as follows:

Reaction 1

$$\log_{10}(k_{rec,0}/\text{cm}^6 \text{ molecule}^{-2} \text{ s}^{-1}) = -23.39 + 1.41 \log T - 0.751 \log^2 T$$

$$k_{rec,\infty} = 7.02 \times 10^{-10} \exp(-38.4/T) \text{ cm}^3 \text{ molecule}^{-1} \text{ s}^{-1}$$

$$F_c = 0.31$$

Reaction 2

$$\log_{10}(k_{rec,0}/\text{cm}^6\ \text{molecule}^{-2}\ \text{s}^{-1}) = -36.14 + 9.24 \log T - 2.19 \log^2 T$$

$$k_{rec,\infty} = 7.97 \times 10^{-10} \exp(-190/T)\ \text{cm}^3\ \text{molecule}^{-1}\ \text{s}^{-1}$$

$$F_c = 0.36$$

Reaction 3

$$\log(k_{rec,0}/\text{cm}^6\ \text{molecule}^{-2}\ \text{s}^{-1}) = -42.19 + 13.15 \log T - 2.87 \log^2 T$$

$$k_{rec,\infty} = 9.90 \times 10^{-10} \exp(-195/T)\ \text{cm}^3\ \text{molecule}^{-1}\ \text{s}^{-1}$$

$$F_c = 0.43$$

The uncertainty involved in using the above expressions to extrapolate k_{rec} outside the experimental range of temperature and pressure was estimated using the following procedure. The effect of seven parameters was considered: A^∞, E^∞, $\langle\Delta E\rangle_{down}$, α, σ (the adduct-N_2 collision cross-section), the adduct binding energy, and the lowest vibrational frequency of the adduct. The individual uncertainty of each of these parameters was assigned to be that which caused χ^2 in eq V to double. A set of the seven parameters was then chosen by Monte Carlo sampling of each parameter, assuming a uniformly random distribution within each parameter's range of uncertainty. k_{calc} was then calculated at three temperatures over the experimental pressure range. If k_{calc} fell within $\pm$ 20% of k_{expt}, then this set of parameters was used to extrapolate k_{calc} to a chosen temperature and pressure. This criterion allows for the fact that the fitted parameters are not all independent of each other. The procedure was repeated until 200 successful Monte Carlo selections and extrapolations had been performed. The uncertainty in the extrapolated k_{calc} is then given by 2 standard deviations about the mean of the 200 estimates. This approach is a simplified (and less computer-intensive) variation on the Monte Carlo technique developed by Hessler.[35]

Over the temperature range from 200 to 600 K, the following uncertainties are estimated. For reaction 1, 80% uncertainty in k_1 for $P < 0.1$ Torr, 40% for $0.1 < P < 10$ Torr, and 20% for $10 < P < 10^3$ Torr. For reaction 2, 40% uncertainty in k_2 at $P < 0.1$ Torr, and 25% for $0.1 < P < 10^3$ Torr. For reaction 3, 30% uncertainty in k_3 for $P < 0.1$ Torr, 20% for $0.1 < P < 10$ Torr, and 30% for $10 < P < 10^3$ Torr. For the particular case of upper mesospheric conditions of temperature (120−240 K) and pressure at 85 km ($\sim 3 \times 10^{-3}$ Torr), the resulting uncertainties in k_{1-3} are illustrated in Figure 9.

The only comparison that can be made with previous experimental work on CaO is an estimate for k_1 from a study of catalysis of flame radical recombination by Jensen and Jones.[7] This indicated a second-order rate coefficient of about 6×10^{-10} cm^3 $molecule^{-1}$ s^{-1} at a pressure of 1 atm and a temperature of about 2000 K.[36] Using the RRKM fit described above to extrapolate the present experimental data to these flame conditions, we obtain a value of 6.2×10^{-10} cm^3 $molecule^{-1}$ s^{-1}, in apparently excellent agreement with the flame result, although this had a large assigned uncertainty.[36]

Finally, it is interesting to compare the rates of these reactions with the limited data available on the analogous reactions of other metal oxide molecules. The low-pressure limiting rate coefficients for the recombination of FeO with H_2O, CO_2, and O_2 are respectively about 3, 4, and 2 orders of magnitude slower than the CaO reactions 1−3, over the temperature range 200−500 K. These marked differences in rate coefficients arise mostly because the binding energies of FeO with these reactants are considerably smaller than for CaO, particularly for FeO + CO_2.[15] The reactions of NaO with CO_2 and O_2 are slower by factors of 5 and 200 at 300 K than the analogous CaO reactions.[37] Once again, even though NaO is a radical, it binds relatively weakly to these molecules.[38] Note that NaO does not recombine with H_2O, but produces NaOH by abstraction.[38,39]

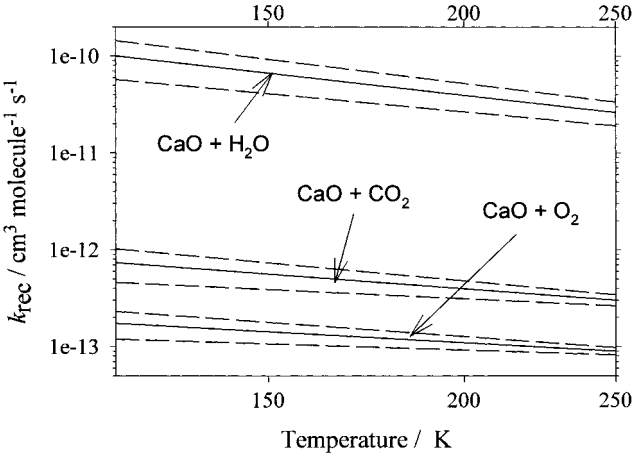

Figure 9. Recombination rate coefficients for the recombination between CaO and H_2O, CO_2 and O_2 extrapolated using RRKM theory to mesospheric temperatures and pressure (0.003 Torr). The broken lines indicate the 2σ uncertainty, estimated using the Monte Carlo procedure described in the text.

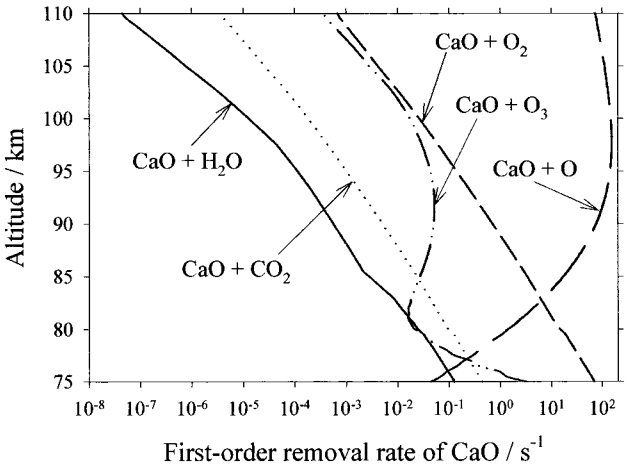

Figure 10. First-order removal rates for CaO in the upper mesosphere. Conditions are January, 40°N (see ref 41 for further details on the profiles of temperature and the concentrations of minor species).

Atmospheric Implications. Figure 10 shows altitude profiles of the removal rates of CaO by reactions 1−4, as well as by reaction with atomic O

$$\text{CaO} + \text{O} \rightarrow \text{Ca} + \text{O}_2 \qquad (7)$$

We have previously measured k_7 to be 6.5×10^{-10} cm^3 $molecule^{-1}$ s^{-1} at 805 K;[40] to extrapolate down to mesospheric temperatures, we assume that this rapid rate coefficient has a small ($T^{1/2}$) temperature dependence giving $k_7(200\ \text{K}) = 3.2 \times 10^{-10}$ cm^3 $molecule^{-1}$ s^{-1}. Although reaction 7 dominates CaO removal, the resulting Ca is rapidly re-oxidized by O_3 (reaction 5).[6] Hence, the formation of reservoir calcium compounds must occur through reactions 1−4. Using the heats of formation for the calcium species listed in Table 5 (adopting the experimental

value for CaO[20]), taking $\Delta H_{f,0}^{o}(CaO_2(^1A_1)) = -51.6$ kJ mol^{-1} and $\Delta H_{f,0}^{o}(CaO_2(^3A_2)) = -17.8$ kJ mol^{-1},[10] and other heats of formation from ref 19, the following spin-allowed reactions are exothermic and could therefore be significant in the upper mesosphere (ΔH_0^o/kJ mol^{-1}, provided in parentheses, uncertainty $\pm$ 20 kJ mol^{-1}):

$$CaO_2(^1A_1) + O \rightarrow CaO + O_2 \quad (-170) \quad (8)$$

$$CaO_2(^1A_1) + H \rightarrow CaOH + O \quad (-94) \quad (9)$$

$$CaO_2(^1A_1) + O_3 \rightarrow OCaO_2(^3A') + O_2 \quad (-281) \quad (10)$$

$$OCaO_2(^3A') + O \rightarrow CaO_2(^3A_2) + O_2 \quad (-77) \quad (11)$$

$$OCaO_2(^3A') + H \rightarrow CaOH + O_2 \quad (-204) \quad (12)$$

$$OCaO_2(^3A') + H_2O \rightarrow Ca(OH)_2 + O_2 \quad (-181) \quad (13)$$

$$CaCO_3 + O \rightarrow CaO_2(^3A_2) + CO_2 \quad (-43) \quad (14)$$

$$CaCO_3 + H \rightarrow CaOH + CO_2 \quad (-170) \quad (15)$$

$$CaCO_3 + H_2O \rightarrow Ca(OH)_2 + CO_2 \quad (-148) \quad (16)$$

$$Ca(OH)_2 + H \rightarrow CaOH + H_2O \quad (-23) \quad (17)$$

$$CaOH + H \rightarrow Ca + H_2O \quad (-102) \quad (18)$$

$$CaOH + H \rightarrow CaO + H_2 \quad (-15) \quad (19)$$

These reactions do not appear to have been studied previously, apart from estimates for k_{17}, k_{18}, and k_{19} from a flame study by Jensen and Jones.[7,36] The flame result for reaction 17 implies that this reaction is quite slow at 200 K, so that $Ca(OH)_2$ is probably the major atmospheric reservoir for calcium immediately below the atomic Ca layer. Although Figure 10 shows that its direct formation through reaction 1 is comparatively slow in the mesosphere, $Ca(OH)_2$ probably forms indirectly by $OCaO_2$ and $CaCO_3$ reacting with H_2O (reactions 13 and 16). $OCaO_2$ forms very rapidly below about 85 km (which is where the lower boundary of the Ca layer occurs[1,4,5]), both through reaction 3 and also probably by the sequential oxidation of CaO by O_3 (reaction 4 followed by reaction 10).

Our recent model[1] of mesospheric calcium assumes this scenario with $Ca(OH)_2$ as the major reservoir, and is able to reproduce satisfactorily the characteristic features of the atomic Ca layer, including its unusual seasonal behavior. However, recent ab initio calculations that we have carried out indicate that CO_2 can add sequentially to $Ca(OH)_2$ to form $Ca(HCO_3)_2$, which is stable even to reaction with atomic H. This dibicarbonate is probably the major sink for calcium further down in the mesosphere. The results of these calculations will be published elsewhere.

Acknowledgment. This work and a research studentship for R.J.R. were supported by the Natural Environment Research Council's program *Laboratory Studies in Atmospheric Chemistry* (Grant No. GST/02/1242). We thank Dr. P. D. Siders for communicating the results of his calculations on calcium carbonate.

References and Notes

(1) Gerding, M.; Alpers, M.; von Zahn, U.; Rollason, R. J.; Plane, J. M. C. *J. Geophys. Res.* **2000**, *105*, 27 131.

(2) Plane, J. M.C. *Int. Rev. Phys. Chem.* **1991**, *10*, 55.

(3) von Zahn, U.; Gerding, M.; Höffner, J.; McNeil, W. J.; Murad, E. *Meteor. Planetary Sci.* **1999**, *34*, 1017.

(4) Granier, C.; Jegou, J. P.; Megie, G. *J. Geophys. Res.* **1989**, *94*, 9917.

(5) Qian, J.; Gardner, C. S. *J. Geophys. Res.* **1995**, *100*, 7453.

(6) Helmer, M.; Plane, J. M. C.; Allen, M. R. *J. Chem. Soc., Faraday Trans.* **1993**, *89*, 763.

(7) Jensen, D. E.; Jones, G. A. *Proc. R. Soc. London* **1978**, *A 364*, 509.

(8) (a) Thomas, D. M.; Andrews, L. *J. Mol. Spectrosc.* **1974**, *50*, 220. (b) Ault, B. S.; Andrews, L. *J. Phys. Chem.* **1975**, *62*, 2320.

(9) Andrews, L.; Chertihin, G. V.; Thompson, C. A.; Dillon, J.; Byrne, S.; Bauschlicher, C. W., Jr. *J. Phys. Chem.* **1996**, *100*, 10 088.

(10) Cambell, M. L.; Plane, J. M. C. *J. Phys. Chem. A.*, in press.

(11) De Avillez Pereira, R.; Baulch, D. L.; Pilling, M. J.; Robertson, S. H.; Zeng, G. *J. Phys. Chem.* **1997**, *101*, 9681.

(12) Paternack, L.; Dadgidian, P. J. *Chem. Phys.* **1978**, *33*, 1.

(13) DeMore, W. B.; Sander, S. P.; Golden, D. M.; Hampson, R. F.; Kurylo, M. J.; Howard, C. J.; Ravishankara, A. R.; Kolb, C. E.; Molina, M. J. *Chemical Kinetics and Photochemical Data for Use in Stratospheric Modeling: Evaluation 12*; Jet Propulsion Laboratory, California, 1997.

(14) Plane, J. M. C.; Rollason, R. J. *Phys. Chem. Chem. Phys.* **1999**, *1*, 1843.

(15) Rollason, R. J.; Plane, J. M. C. *Phys. Chem. Chem. Phys.* **2000**, *2*, 2335.

(16) Nien, C.-F.; Rajasekhar, B.; Plane, J. M. C. *J. Phys. Chem.* **1993**, *97*, 6449.

(17) Frisch, M. J.; Trucks, G. W.; Schlegel, H. B.; Scuseria, G. E.; Robb, M. A.; Cheeseman, J. R.; Zakrzewski, V. G.; Montgomery, J. A., Jr.; Stratmann, R. E.; Burant, J. C.; Dapprich, S.; Millam, J. M.; Daniels, A. D.; Kudin, K. N.; Strain, M. C.; Farkas, O.; Tomasi, J.; Barone, V.; Cossi, M.; Cammi, R.; Mennucci, B.; Pomelli, C.; Adamo, C.; Clifford, S.; Ochterski, J.; Petersson, G. A.; Ayala, P. Y.; Cui, Q.; Morokuma, K.; Malick, D. K.; Rabuck, A. D.; Raghavachari, K.; Foresman, J. B.; Cioslowski, J.; Ortiz, J. V.; Baboul, A. G.; Stefanov, B. B.; Liu, G.; Liashenko, A.; Piskorz, P.; Komaromi, I.; Gomperts, R.; Martin, R. L.; Fox, D. J.; Keith, T.; Al-Laham, M. A.; Peng, C. Y.; Nanayakkara, A.; Gonzalez, C.; Challacombe, M.; Gill, P. M. W.; Johnson, B.; Chen, W.; Wong, M. W.; Andres, J. L.; Gonzalez, C.; Head-Gordon, M.; Replogle, E. S.; Pople, J. A. *Gaussian 98, Revision A.7*, Gaussian, Inc., Pittsburgh, PA, 1998.

(18) Foresman, J. B.; Frisch, A. *Exploring Chemistry with Electronic Structure Methods*; Gaussian, Inc.: Pittsburgh, PA, 1996.

(19) Chase, M. W.; Davies, C. A.; Downey, J. R.; Frurip, D. J.; McDonald, R. A.; Syverud, A. N. JANAF Thermochemical Tables, 3rd ed.; *J. Phys. Chem. Ref. Data*, **1985**, *14*.

(20) Schofield, K. S. In *Gas-Phase Metal Reactions*; Fontijn, A., Ed.; Elsevier: Amsterdam, 1992, pp 529−571.

(21) Steimle, T. C.; Fletcher, D. A.; Jung, K. Y.; Scurlock, C. T. *J. Chem. Phys.*, **1992**, *96*, 2556.

(22) Bernath, P. F.; Kinsey-Nielsen, S. *Chem. Phys. Lett.* **1984**, *105*, 663.

(23) Coxon, J. A.; Li, M.; Presunka, P. I. *J. Mol. Phys.* **1994**, *164*, 118.

(24) Jarman, C. N.; Bernath, P. F. *J. Chem. Phys.* **1992**, *97*, 1711.

(25) Kauffman, J. W.; Hauge, R. H.; Margrave, J. L. *High Temp. Sci.* **1984**, *17*, 237.

(26) Langhoff, S. R.; Bauschlicher, C. W., Jr.; Partridge, H. *J. Chem. Phys.* **1986**, *84*, 4474.

(27) Bauschlicher, C. W., Jr.; Langhoff, S. R.; Steimle, T. C.; Shirley, J. E. *J. Chem. Phys.* **1990**, *93*, 4179.

(28) Thackeray, D. J.; Siders, P. D. *J. Chem. Soc., Faraday Trans.* **1998**, *94*, 2653.

(29) Maitland, G. C.; Rigby, M.; Brian Smith, E.; Wakeham, W. A. *Intermolecular Forces: Their Origin and Determination*; Oxford University Press: Oxford, **1987**.

(30) *Handbook of Physics and Chemistry*; Lide, D. R., Ed.; CRC Press: Boca Raton, 78th. ed., 1997.

(31) Murad, E. *J. Chem. Phys*. **1983**, *78*, 6611.
(32) Lias, S. G.; Bartmess, J. E.; Liebman, J. F.; Holmes, J. L.; Levin, R. D.; Mallard, W. G.; Gas-Phase Ion and Neutral Thermochemistry; *J. Phys. Chem. Ref. Data* **1988**, *17*.
(33) Gilbert, R. G.; Smith, S. C. *Theory of Unimolecular and Recombination Reactions*, Blackwell, Oxford, 1990.
(34) Troe, J. *J. Chem. Phys.* **1977**, *66*, 4758.
(35) Hessler, J. P. *Int. J. Chem. Kinet.* **1997**, *29*, 803.
(36) Jensen, D. E.; Jones, G. A. *Combust. Flame* **1978**, *32*, 1.
(37) Ager, J. W.; Howard, C. J. *Geophys. Res. Lett.* **1986**, *13*, 1395.
(38) Ager, J. W.; Howard, C. J. *J. Chem. Phys.* **1987**, *87*, 921.
(39) Cox, R. M.; Plane, J. M. C. *Phys. Chem. Chem. Phys.* **1999**, *1*, 4713.
(40) Plane, J. M. C.; Nien, C.-F. *J. Phys. Chem.* **1990**, *94*, 5255.
(41) Plane, J. M. C.; Gardner, C. S.; Yu, J.; She, C. Y.; Garcia, R. R.; Pumphrey, H. C. *J. Geophys. Res.* **1999**, *104*, 3773.